The Astrophysical Journal, 992:179 (9pp), 2025 October 20 https://doi.org/10.3847/1538-4357/ae0991

Evolution of Low Surface Brightness Ultrathin Galaxies: The Role of Dark Matter Halo and Bar Formation on Disk Thickness

K. Aditya[1,2] and Arunima Banerjee[3]
[1] Raman Research Institute, C. V. Raman Avenue, 5th Cross Road, Sadashivanagar, Bengaluru, 560080, India
[2] Indian Institute of Astrophysics, Koramangala, Bengaluru 560 034, India
[3] Department of Physics, Indian Institute of Science Education and Research (IISER), Tirupati—517507, India
Received 2025 April 8; revised 2025 September 10; accepted 2025 September 12; published 2025 October 14

Abstract

We investigate how stellar disks sustain their ultrathin structure throughout their evolution. We follow the evolution of ultrathin stellar disks with varying dark matter (DM) halo concentration (c) using collisionless N-body simulations with AREPO. We test models embedded in steep ($c = 12$), shallow ($c = 2$), and intermediate ($c = 6$) DM concentrations. Our models match the observed structural properties of the stellar disk in the low surface brightness (LSB) ultrathin galaxy FGC 2366, specifically its surface brightness, disk scalelength, and vertical thinness ($h_z/R_D = 0.1$), while excluding gas, allowing us to isolate the effects of DM. The internal disk heating mechanism driven by bars is suppressed in the LSB ultrathin stellar disks regardless of the DM concentration. The ratio of disk thickness (h_z) to scalelength (R_D) remains constant at $\leqslant 0.1$ throughout their evolution. To clearly establish that the LSB nature of stellar disks is the key to preventing disk thickening, we construct the initial conditions by increasing the stellar mass fraction from $f_s \sim 0.01$ to 0.02 and 0.04, respectively, while keeping the total mass equal to $10^{11} M_\odot$ and $h_z/R_D \leqslant 0.1$ unchanged. We find that models with a higher stellar mass fraction embedded in a shallow DM potential ($c = 2$) form bars and undergo significant disk thickening ($h_z/R_D \gg 0.1$) concurrent with the bar growth. We conclude that if the LSB disks are thin to begin with, they remain so throughout their evolution in isolation, regardless of the concentration of the DM halo.

Unified Astronomy Thesaurus concepts: Galactic and extragalactic astronomy (563)

1. Introduction

Ultrathin galaxies (UTGs) are late-type edge-on disk galaxies characterized by a large major-to-minor-axis ratio ($a/b > 10$; J. W. Goad & M. S. Roberts 1981; L. Matthews et al. 1999; K. Aditya et al. 2022, 2023). UTGs lack a discernible bulge component and exhibit low surface brightness (LSB), with central surface brightness in B-band, $\mu_B > 22.5$ mag arcsec^{-2} (S. S. McGaugh 1996; G. Bothun et al. 1997). Although ubiquitous in observations (I. D. Karachentsev et al. 1999; S. Kautsch et al. 2006; D. Bizyaev et al. 2017, 2021), UTGs are notably rare in ΛCDM simulations. M. Haslbauer et al. (2022), measured the sky-projected aspect ratio distribution in the ΛCDM simulations IllustrisTNG (M. Vogelsberger et al. 2014; A. Pillepich et al. 2018) and EAGLE (J. Schaye et al. 2015), and they found that these simulations are deficient in galaxies with intrinsically thin disks. Additionally, C. Bottrell et al. (2017) show that these simulations are deficient in bulge-dominated low-mass galaxies. However, more recent studies by J. Hu et al. (2024) and D. Xu et al. (2024) show that there is no shortage of thin-disk galaxies in TNG-50. It is now well established that the bars and spiral arms (K. Saha 2014; M. Aumer et al. 2016; R. J. Grand et al. 2016) can significantly heat the stellar disks radially, and giant molecular clouds (A. Jenkins & J. Binney 1990) can heat the stellar disks radially and isotropically. However, the minimal vertical thickness indicates a negligible effect of disk heating agents in UTGs. Thus, the formation, evolution, and sustenance of these extremely thin stellar disks in UTGs remain a mystery and challenge our current understanding of galaxy formation and evolution models.

UTGs are distinguished by their extreme structural and photometric properties and characterized by equally extreme kinematic and dynamical features. A. Komanduri et al. (2020) and K. Aditya & A. Banerjee (2021) have shown UTGs have central vertical velocity dispersion ($\sigma_{0s} = 10$ km s^{-1}–18 km s^{-1}) comparable to the thin stellar disk in the Milky Way (S. Sharma et al. 2014). Additionally, UTGs are dynamically stable against the growth of axisymmetric instabilities (K. Aditya & A. Banerjee 2021; K. Aditya et al. 2022, 2023), which may explain the low star formation rates observed in these galaxies (G. Narayanan & A. Banerjee 2021). Furthermore, UTGs have a higher specific angular momentum compared to the ordinary spiral galaxies (Y. V. Jadhav & A. Banerjee 2019; K. Aditya et al. 2022, 2023), indicating that these galaxies rotate faster than ordinary spiral galaxies for a given stellar mass. It has been demonstrated that the extreme flattening of UTGs can be attributed to a compact and dense dark matter (DM) halo (A. Banerjee & C. J. Jog 2013). This finding is further supported by DM models based on H I 21 cm synthesis observations of two of the thinnest known galaxies, FGC 1440 ($a/b = 20$) and FGC 2366 ($a/b = 22$; K. Aditya et al. 2022, 2023). These results suggest that the DM halo plays an important role in regulating the vertical structure of galaxies hosting extremely thin stellar disks.

Previous studies have shown that bar formation in LSB galaxies is closely tied to the mass distribution of the stellar and DM components. Numerical simulations of LSB galaxies indicate that bar formation requires a disk mass at least twice as high as typically inferred for LSBs (L. Mayer & J. Wadsley 2004). Disks with low surface density are generally stable against bar formation, especially within halos with relatively higher DM concentration. Similarly, simulations by J. A. Sellwood & N. W. Evans (2001) show that a stellar disk embedded in a DM halo with a large core radius is stable to $m = 2$ modes (S. M. Fall & D. Lyndon-Bell 1981). This is further corroborated

Table 1
Structural Parameters Derived from Optical Photometry of FGC 2366

Parameters Galaxy	Σ_0 ($M_\odot$ pc^{-2})	R_D (kpc)	h_z (kpc)	a/b
FGC 2366	24.1	2.6	0.29	21.6

in the numerical work by S. Ghosh & C. J. Jog (2014), who show that a dominant DM halo can suppress the formation of both axisymmetric and nonaxisymmetric instabilities like bars and spiral formation in the prototypical LSB UTG UGC 7321. Besides, cosmological simulations show that LSBs often inhabit halos with relatively low central density (J. Bailin et al. 2005) or high spin (L. E. Pérez-Montaño et al. 2022; K. Chim-Ramirez et al. 2025), yielding extended stellar disks with low central densities. K. Chim-Ramirez et al. (2025) show that the lower bar fraction in LSBs in the TNG-100 simulations is associated with their higher spin and gas content, factors known to inhibit bar formation and growth.

While previous studies have addressed the influence of DM on the vertical structure of UTGs using semianalytic models and have probed the connection between bar formation and DM concentration in LSB galaxies, these investigations have largely treated these effects in isolation. The nexus between the shape of the DM halo and the surface brightness of the stellar disk and how they jointly govern the bar formation and ultimately regulate the vertical structure of LSB UTGs hitherto remain unexplored.

In the present study, we will perform a series of *N*-body simulations using AREPO (R. Weinberger et al. 2020) to investigate the following question: how do stellar disks sustain their ultrathin structure throughout their evolution? We will describe the initial conditions in Section 2 and present the results from the analysis of the *N*-body simulations in Section 3. Finally, we will conclude in Section 4.

2. Initial Conditions

We use FGC 2366 as a template for constructing the initial conditions corresponding to the various models of UTGs presented in the study. FGC 2366 is the thinnest known galaxy, with an extraordinarily large major-to-minor-axis ratio ($a/b \approx 22$). The stellar photometry, total rotation curve, and DM models for FGC 2366 are available in K. Aditya et al. (2023). We construct the initial condition corresponding to FGC 2366 using the Disk Initial Conditions Environment (V. Perret 2016). The structural parameters of the stellar disk are presented in Table 1. The stellar surface density is given by

$$\Sigma_s(R, z) = \Sigma_0 e^{-\left(\frac{R}{R_D}\right)} e^{-\left(\frac{z}{h_z}\right)}, \quad (1)$$

where Σ_0 is the central stellar surface density and R_D and h_z are the exponential stellar disk scalelength and disk scale-height, respectively. The DM is modeled using Navarro–Frenk–White (NFW; J. F. Navarro et al. 1997) profile given by

$$\rho_{\rm DM}(R) = \frac{\rho_0}{\left(1 + \frac{R}{R_s}\right)^2 \left(\frac{R}{R_s}\right)}, \quad (2)$$

where ρ_0 is the central density and R_s the scalelength of DM halo. The rotation curve due to the NFW DM density is given by

$$V(R) = V_{200} \sqrt{\frac{\ln(1 + cx) - cx/(1 + cx)}{x[\ln(1 + c) - c/(1 + c)]}}, \quad (3)$$

where $x = R/R_{200}$, R_{200} is the radius at which the mean density of the DM halo is 200 times the critical density. V_{200} is the rotation velocity at R_{200} and is equal to $0.73R_{200}$. The concentration parameter is defined as $c = R_{200}/R_s$. The value of R_{200} and c completely specify the NFW DM distribution. We present the values of the concentration parameter and R_{200} used for constructing initial conditions in Table 2. We use the stellar density parameters from Table 1 and the DM halo parameters from Table 2 to construct the initial conditions that reproduce the observed properties of FGC 2366, referred to as `c6` in our study. The surface density of the observed model `c6` corresponds to a central surface brightness of 22.8 mag arcsec^{-2} in the z-band. We derive the mass-to-light ratio in the z-band in order to convert the surface brightness in $L_\odot/{\rm pc}^2$ to the surface density in $M_\odot/{\rm pc}^2$ using the calibration given in E. F. Bell et al. (2003). See K. Aditya et al. (2023) for detailed optical photometry of FGC 2366. The empirical calibration between the color and the mass-to-light ratio in a given band is given as $\log_{10}(M/L) = a_\lambda + b_\lambda$(Color). We use the $g - z$ magnitudes ($g = 15.44$, $z = 14.76$) to derive the color ($g - z = 0.7$) and the values of $a_z = -0.17$ and $b_z = 0.32$ tabulated in E. F. Bell et al. (2003) and find mass-to-light ratio equal to 1.12 in the z-band (K. Aditya et al. 2023). The central surface densities of the other models scale proportionally with their respective stellar mass fractions—see Table 2. It has been shown by Y. V. Jadhav & A. Banerjee (2019) and K. Aditya et al. (2022, 2023) that UTGs have a higher specific angular momentum than ordinary spiral galaxies. We present the values of specific angular momentum for different models in Table 2. Unlike ordinary spiral galaxies, FGC 2366 has a higher specific angular momentum for a given stellar mass (K. Aditya et al. 2023). Similarly, L. E. Pérez-Montaño et al. (2022) found that LSBs in TNG-100 simulations have a higher specific angular momentum than ordinary spirals.

To investigate the role of DM in determining disk thickness, we construct two additional models: one with a lower DM concentration (`c2`), resulting in a shallower rotation curve compared to `c6`, and another with a higher central DM concentration (`c12`), which produces a steeper rotation curve. To clearly establish that LSB is key for preventing disk thickening, we construct initial condition by increasing the stellar mass fraction from $f_s \sim 0.008$, corresponding to the LSB thin disk to 0.02 labeled as (`c2-M1`, `c6-M1`, and `c12-M1`) and 0.04 labeled as (`c2-M2`, `c6-M2`, and `c12-M2`). In all the models, we keep the total mass fixed at $10^{11} M_\odot$. Also, we ensure that all our initial conditions comply with the thin-disk criterion $h_z/R_D \leqslant 0.1$, despite the variation in the DM concentration and stellar mass fraction. All the models have been initialized with 10^6 stellar and DM particles, typical for simulations studying bar formation and disk thickening (J. Sellwood 2013; J. Sellwood & O. Gerhard 2020). We present the initial conditions for our model galaxies in Figure 1 and Table 2. Furthermore, all models in our study are purely collisionless. Previous studies have shown that gas generally inhibits bar formation by facilitating angular momentum exchange between the stellar and gaseous components (E. Athanassoula 2003; K. L. Masters et al. 2012; B. C. Sodi & O. S. García 2017). Thus, using collisionless *N*-body simulations represents a conservative approach for

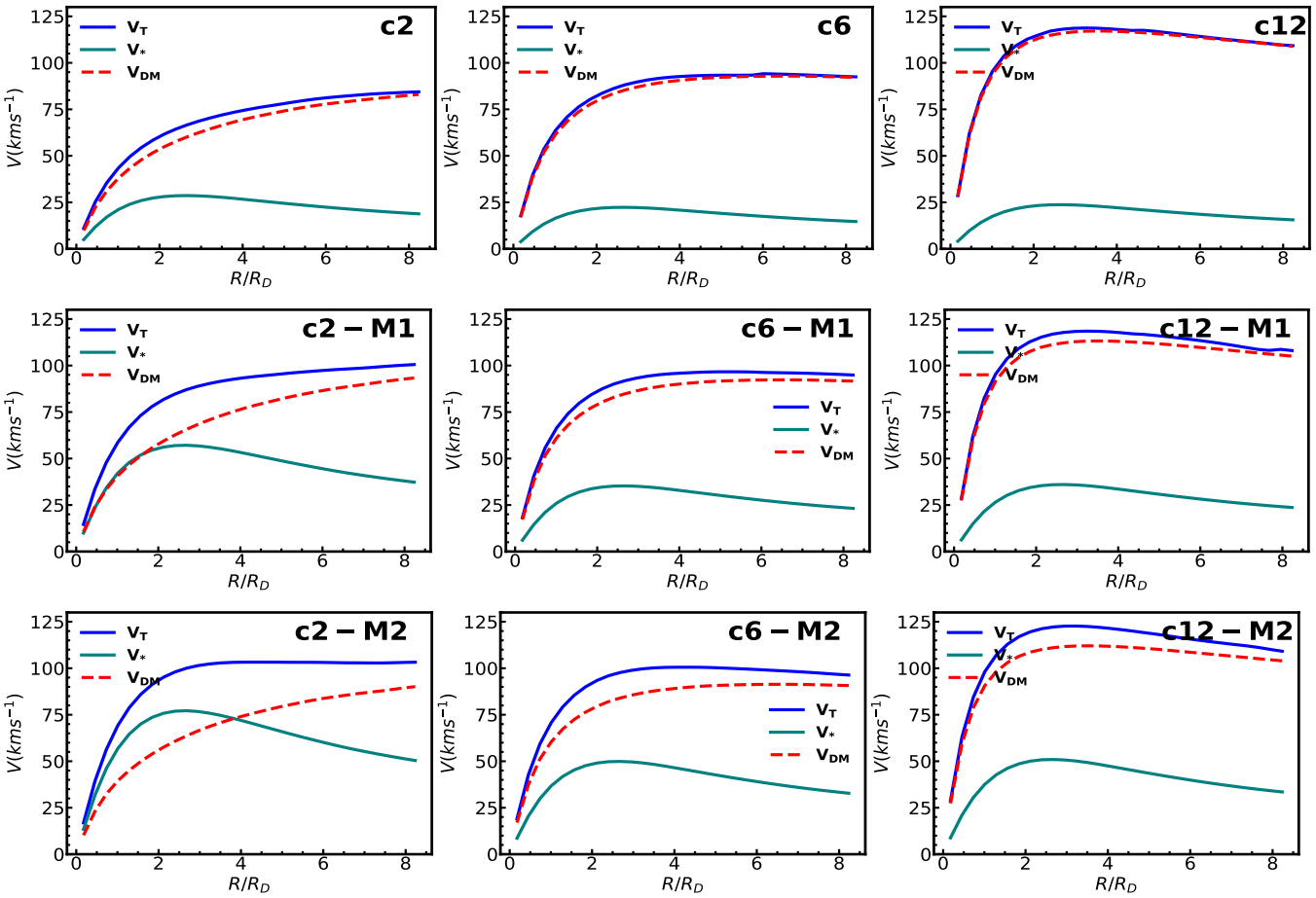

Figure 1. Initial conditions corresponding to various thin-disk models in our study. All the models have a total mass equal to $10^{11} M_{\odot}$ and $h_z/R_D \leqslant 0.1$. The models in the first row with labels `c2`, `c6`, and `c12` have a stellar mass fraction equal to 0.008 and DM concentration equal to 2, 6, and 12, respectively. The model `c6` matches the observed properties of the thinnest known galaxy, FGC 2366. The models in the second row with labels `c2-M1`, `c6-M1`, and `c12-M1` have a higher stellar mass fraction equal to 0.02 and a DM halo concentration indicated by their labels. The models in the third row, labeled as `c2-M2`, `c6-M2`, and `c12-M2`, have the highest stellar mass fraction among our models, equal to 0.04.

Table 2
Initial Conditions for the Simulations

Model	$N_s = N_{\rm DM}$	f_s				$\log(M/M_{\odot})$	c
R_{200}						$\log(j_*/\text{kpc km s}^{-1})$	$\log(\Sigma_0/M_{\odot}\text{kpc}^{-2})$
`c2`	10^6	0.008	11.04	2.1	70.8	2.5	7.6
`c6`	10^6	0.008	10.95	6	62.8	2.6	7.3
`c12`	10^6	0.008	11.02	12	67	2.8	7.4
`c2-M1`	10^6	0.02	11.18	2	83.2	2.6	8.1
`c6-M1`	10^6	0.02	10.95	6	62.5	2.7	7.7
`c12-M1`	10^6	0.02	10.99	12	65	2.8	7.8
`c2-M2`	10^6	0.04	11.16	2	80.4	2.7	8.4
`c6-M2`	10^6	0.04	10.95	6	62	2.7	8.0
`c12-M2`	10^6	0.04	10.99	12	64	2.8	8.1

assessing the role of bar instabilities on the vertical thickness of stellar disks.

3. Results and Discussion

We evolve the initial conditions for different models using the publicly available code AREPO (R. Weinberger et al. 2020). We evolve our initial conditions for 5 Gyr and save the snapshot after every 50 Myr. We show the time evolution of h_z/R_D corresponding to the different models of the ultrathin disks in Figure 2 and the face-on and edge-on projection of the surface density in Figure 3. We quantify the contribution of the internal disk heating due to bars by computing the Fourier amplitude of $m = 2$ modes. The amplitude of the nth Fourier mode at radius R is given by

$$a_n(R) = \sum_{i=1}^{N} m_i(R)\cos(n\theta_i), \quad b_n(R) = \sum_{i=1}^{N} m_i(R)\sin(n\theta_i), \quad (4)$$

where $n = 0, 1, 2, \ldots$ In the above, $m_r(R)$ and θ_i are the mass and the azimuthal angle of the ith particle at radius R and N is the total number of particles at that radial position. The

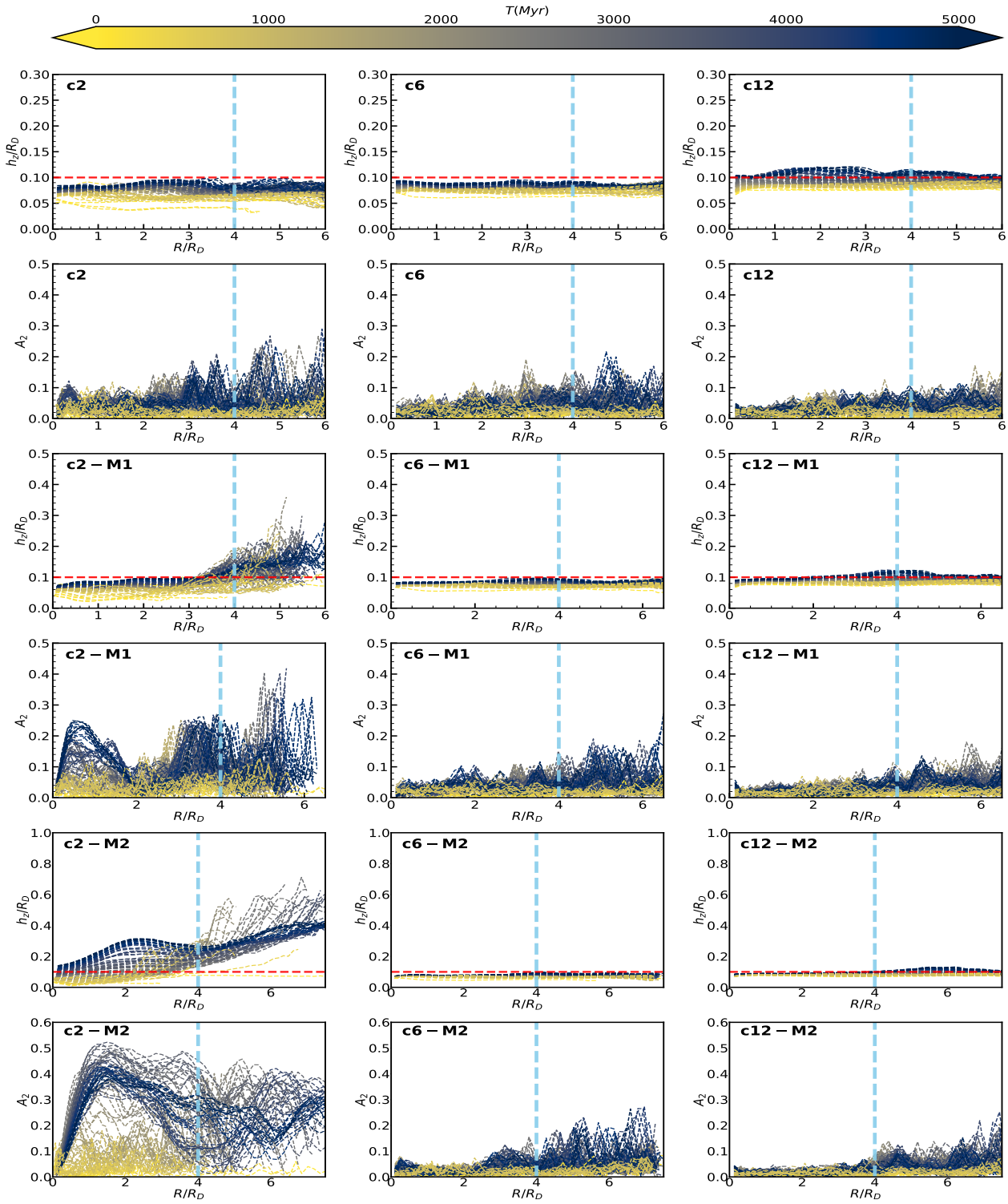

Figure 2. The time evolution of h_z/R_D and the amplitude of the $m = 2$ modes for different models presented in our work. In the top two panels, we show the models `c2`, `c6`, and `c12`, and in the following panels, we show their massive counterparts with a higher stellar mass fraction. We indicate the typical extent of the stellar disk with a vertical dashed line at $4R_D$. The horizontal line indicates the thin-disk criterion: $h_z/R_D = 0.1$.

strength of the nth mode is defined as

$$\frac{A_n}{A_0} = \max\left(\frac{\sqrt{a_n^2 + b_n^2}}{\sum_{i=1}^{N} m_i}\right). \quad (5)$$

Upon inspecting Figure 2, we find that h_z/R_D for `c2`, `c6`, and `c12` at 5 Gyr has hardly changed from its initial value equal to 0.1. Further, from the face-on projections shown in Figure 3 (row 1), we can see that the models `c2`, `c6`, and `c12` do not form bars and that the disks remain thin regardless of the concentration of the DM halo. This highlights the fact that the LSB galaxies do not have sufficient self-gravity to support bar formation. As a result, internal disk heating due to bars is largely suppressed in isolated LSBs, allowing them

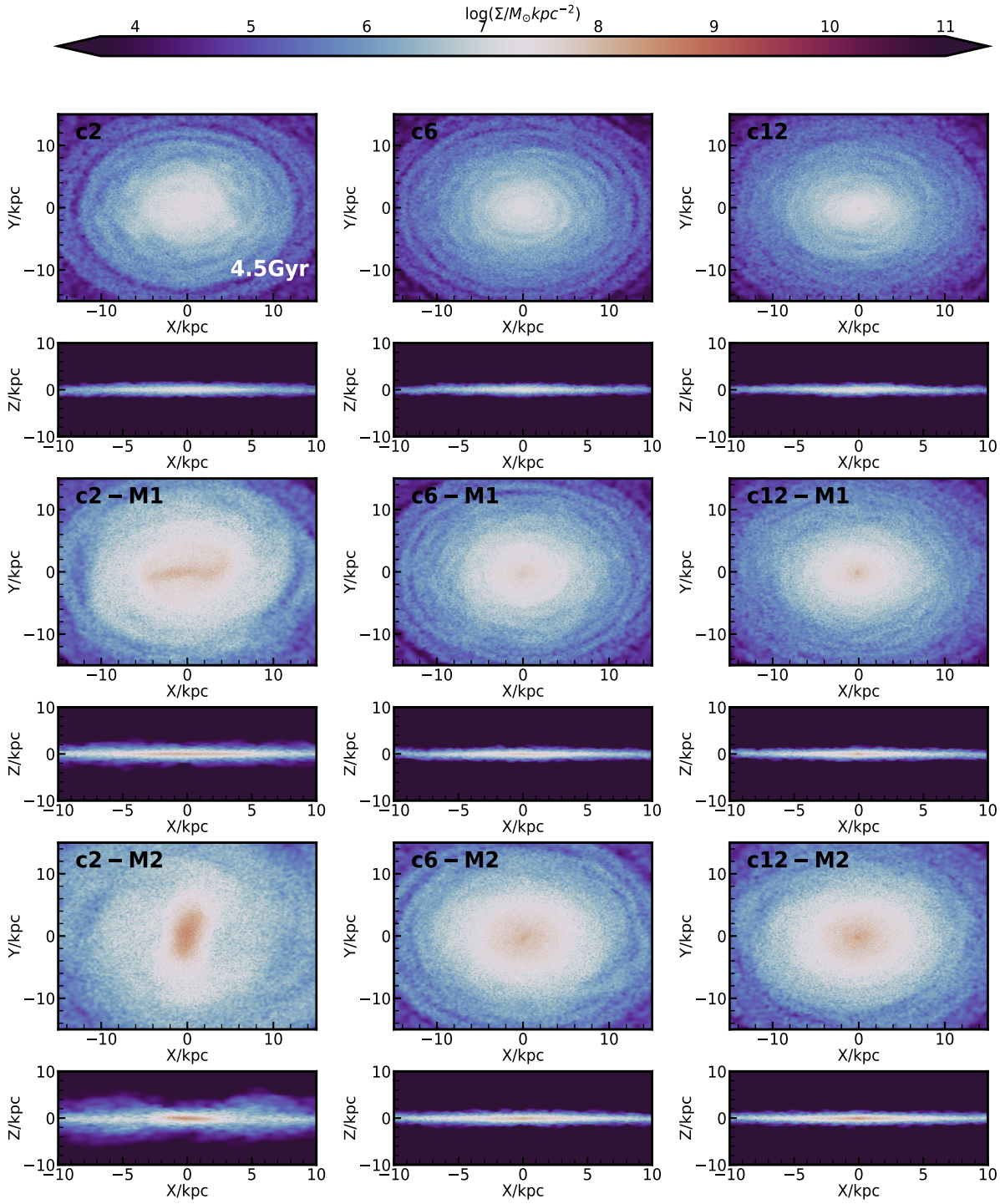

Figure 3. The face-on and the edge-on orientation of the snapshots at $T = 4.5$ Gyr. We show the face-on and the edge-on view corresponding to `c2`, `c6`, and `c12` in the top two panels, respectively, and their massive counterparts with a higher stellar mass fraction in the following panels.

to maintain their ultrathin disk structure throughout their evolution Figure 3 (row 2). Thus, in the LSB models `c2`, `c6`, and `c12`, the shape of the DM halo has little impact on the vertical structure or stellar surface density.

In order to establish that the LSB of the stellar disk is key, we construct another set of initial conditions by increasing the stellar mass fraction from 0.008 to 0.02 (`c2-M1`, `c6-M1`, `c12-M1`) and 0.04 (`c2-M2`, `c6-M2`, `c12-M2`). We find that the models `c2-M1` and `c2-M2` not only form bars but show a significant increase in disk thickness ($h_z/R_D > 0.1$; see Figures 2 and 3). The thickness of the stellar disk in both these models flares with radius. Flaring in the stellar disk is a common feature in massive galaxies; for example, see D. Sotillo-Ramos et al. (2023) for flaring stellar disks in Milky Way analogs in TNG-50. Also, see R. de Grijs & R. F. Peletier (1997) and L. Ossa-Fuentes et al. (2023) for observational evidence of flaring stellar disks. We compare the value of h_z/R_D and A_2 at the end of 5 Gyr for different models in our study in Figure 4. We can see from Figure 4 that the models `c6-M1`, `c12-M1`, `c6-M2`, and `c12-M2` neither form

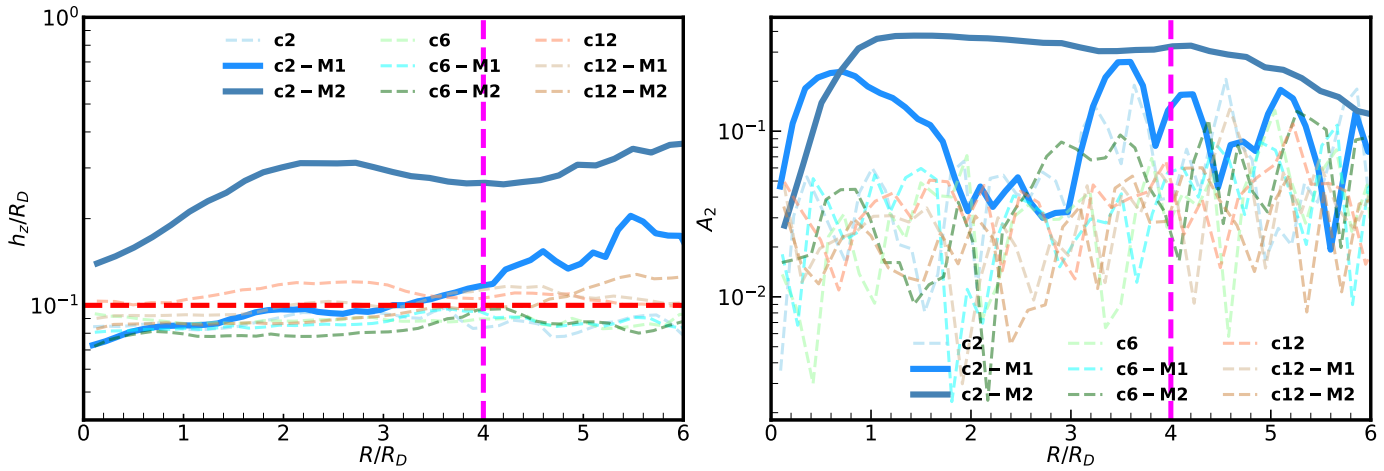

Figure 4. The values of h_z/R_D and the Fourier amplitude of the $m = 2$ mode at $T = 5$ Gyr for different models. The solid lines represent the models `c2-M1` and `c2-M2`, which undergo significant disk heating concurrent with the growth of stellar bars. The other models in the study resist bar formation, thereby evading bar-driven disk thickening. The horizontal line indicates the thin-disk criterion $(h_z/R_D) = 0.1$, and the vertical line represents $4R_D$, beyond which the surface density of the thin disk becomes negligible.

bars nor show signatures of significant disk thickening ($h_z/R_D \not< 0.1$), despite higher self-gravity due to a higher stellar mass fraction. This indicates that the steeper DM potential inhibits bar formation and prevents disk thickening. Previous studies by A. Banerjee & D. Bapat (2017) showed that thin-disk galaxies are embedded in DM halos with steeply rising rotation curves or a steep central DM potential. Our results suggest that the LSB of the stellar disk, in combination with a steep inner DM density profile, is critical for preventing bar-driven disk thickening and maintaining the ultrathin vertical structure. We also note the presence of faint concentric ring-like features in the face-on stellar surface density maps across all models shown in Figure 3.

3.1. Stability of Ultrathin Stellar Disks

In K. Aditya & A. Banerjee (2021) and K. Aditya et al. (2022, 2023), we have shown that UTGs are highly stable with a median stability higher than the nearby spiral galaxies (A. B. Romeo & N. Falstad 2013). A. B. Romeo et al. (2023), K. Aditya (2023, 2024), using a sample of LSBs from the SPARC catalog (F. Lelli et al. 2016) and linear perturbation analysis, show that a rigid DM halo plays an important role in stabilizing LSB galaxies against axis-symmetric instabilities. Using N-body, J. Sellwood (2016) showed that bar instabilities are quelled when the disk is immersed in a massive static DM halo. However, J. Sellwood (2016) also points out that a live halo encourages bar formation. More recent studies by D. Jang & W.-T. Kim (2023) using N-body simulations of Milky Way–type galaxies showed that the bar formation critically depends on the central mass concentration (CMC) and the minimum values of the Toomre stability criterion ($Q_{\rm min}$; A. Toomre 1964), given by

$$(Q_{\rm min}/1.2)^2 + ({\rm CMC}/0.05)^2 \leqslant 1. \quad (6)$$

D. Jang & W.-T. Kim (2023) in their study model the DM halo using a Hernquist profile (L. Hernquist 1990), compared to the NFW DM profile used in our study. Furthermore, the galaxy models considered by D. Jang & W.-T. Kim (2023) have stellar and DM components comparable in size and mass to those of the Milky Way and include a varying CMC. In comparison, our models represent LSBs with structural properties that match those of FGC 2366, the thinnest known disk galaxy. I. Karachentsev et al. (1993) and L. Matthew et al. (2000) show that UTGs by definition are bulgeless systems. Further, optical photometry by K. Aditya et al. (2023) reveals that FGC 2366 does not host a stellar bulge. Since our UTG models are based on the structural parameters of FGC 2366, which lacks a central bulge component, the bar formation criterion suggested by D. Jang & W.-T. Kim (2023) is just $Q_{\rm min} \leqslant 1.4$. We show the time evolution of Q for our models of UTGs in Figure 5. All the ultrathin LSB models that do not form bars—`c2`, `c6`, and `c12`—have $Q > 1.4$. We find that the thin-disk models `c2-M1` and `c2-M2`, which form bars and undergo disk thickening, have $Q_{\rm min} < 1.4$. Further, we note that models with steep inner DM halo have $Q_{\rm min} > 1.4$ and do not form bars. Indirectly, $Q_{\rm min} > 1.4$ suggests that UTGs in our study are not susceptible to disk thickening driven by bars.

3.2. Efstathiou–Lake–Negroponte Criterion

G. Efstathiou et al. (1982) investigated the global stability of disk galaxies using N-body experiments and showed that the models with

$$X = \frac{V_{\rm max}}{(GM_D/R_D)^{1/2}} \leqslant 1.1 \quad (7)$$

favor bar formation. In the above equation $V_{\rm max}$, M_D, and R_D are the maximum circular velocity, the mass of the stellar disk, and the disk scalelength. We show X as a function of time for all our galaxies in Figure 6. We can see that all our models except `c2-M1` and `c2-M2` have $X > 1.1$. The models `c2-M1` and `c2-M2` not only have $Q_{\rm min} < 1.4$ but also satisfy $X < 1.1$. The models `c2-M1` and `c2-M2` have a higher stellar mass fraction and hence higher self-gravity, which supports bar formation. However, models with higher DM concentration do not form bars despite having a higher stellar mass fraction. This occurs because when the DM concentration is lowered while keeping the total mass constant, the reduced central DM mass is compensated by a higher stellar mass in the central regions. Thus, the shallow DM potential does not provide

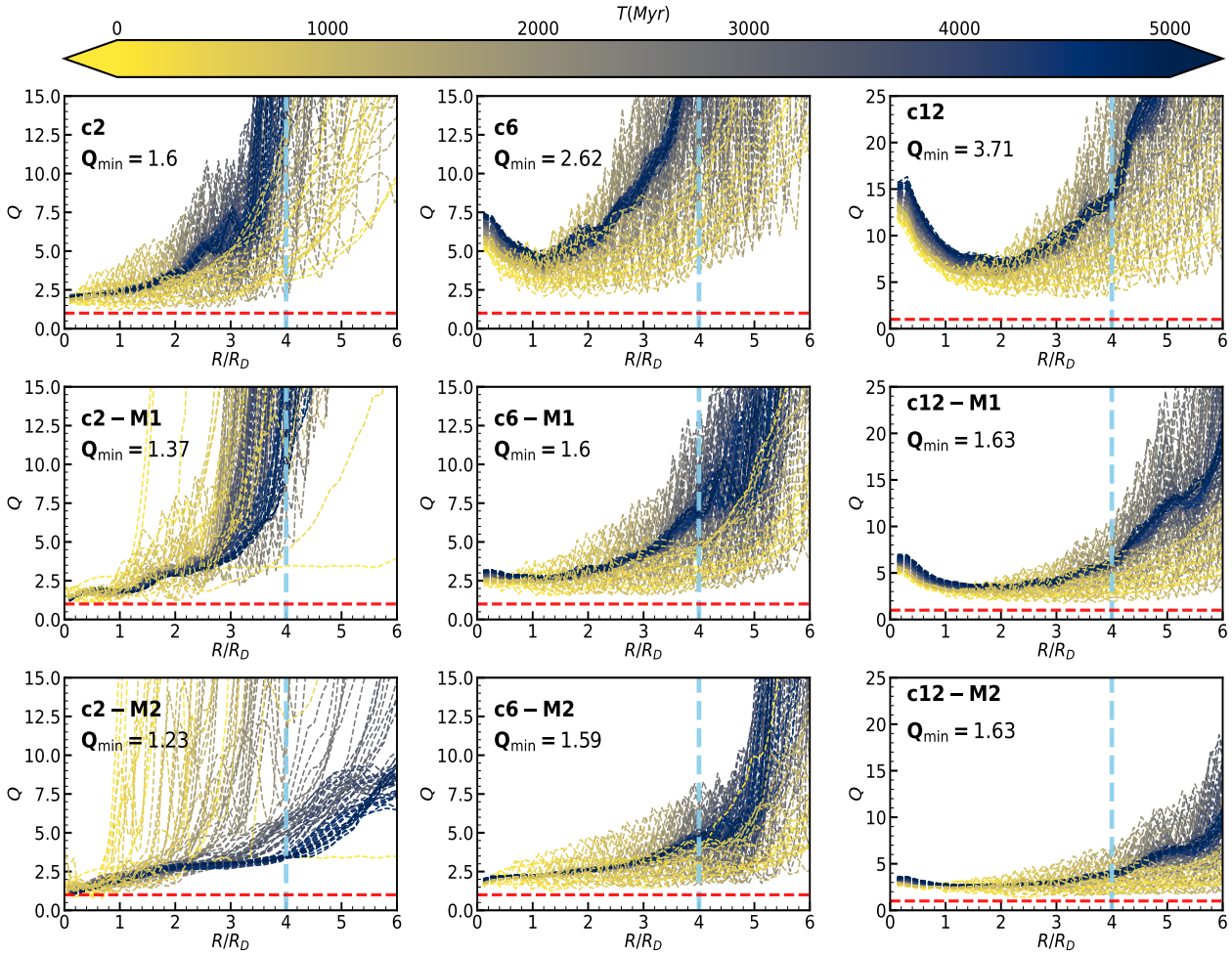

Figure 5. The time evolution of the stability criterion Q. In the top two panels, we show the models `c2`, `c6`, and `c12`, and in the following panels, we show their massive counterparts with a higher stellar mass fraction. We indicate the typical extent of the stellar disk with a vertical dashed line at $4R_D$. The horizontal line indicates the criterion for marginal stability: $Q = 1$.

sufficient centrifugal support to counteract the increased self-gravity of the stellar disk in the central regions, leading to $X < 1.1$ and eventually resulting in disk thickening driven by bar formation. However, the steeper DM potential provides significant centrifugal support and stabilizes the ultrathin stellar disk against bar formation.

4. Conclusions

The results presented in this work show that the collisionless models of LSB ultrathin stellar disks do not form bars and that the disks remain thin regardless of the concentration of the DM halo. The initial disk scaleheight ratio, h_z/R_D, remains nearly constant, suggesting that the LSB ultrathin stellar disks are highly resistant to internal heating mechanisms due to bars and spiral arms, which typically drive vertical heating and disk thickening (K. Saha et al. 2010; J. Sellwood & O. Gerhard 2020; S. Ghosh et al. 2024). Furthermore, upon increasing the mass fraction, we find that the ultrathin stellar disks embedded in a shallow DM halo undergo disk thickening concurrent with bar formation. In contrast, a steep DM halo stabilizes the ultrathin stellar disks against bar formation even with a higher stellar mass fraction.

We note, however, that our models do not include gas and hence are not ideal analogs of FGC 2366. They are constructed to match the observed structural parameters of the galaxy, such as the stellar surface density, scalelength, and thickness of the stellar disk. Our models consider only the stellar disk embedded in a DM halo, since our aim here was to isolate the dynamical effect of DM halo concentration on bar formation and eventually on the vertical thickness of stellar disks.

Several studies have shown that the presence of gas can suppress bar formation. For instance, observational studies by K. L. Masters et al. (2012), B. C. Sodi & O. S. García (2017), and Z. Zhou et al. (2021) suggest that angular momentum exchange between stars and gas inhibits bar growth (see also E. Athanassoula 2003). Likewise, a recent study by K. C. Ramirez et al. (2025), using TNG-100 simulations, shows that LSB galaxies with stellar mass below $10^{11} M_\odot$ exhibit a consistently lower bar fraction than high surface brightness galaxies, which could be attributed to their higher gas fractions. So, although we have not included gas in our models, the available evidence suggests that doing so would have further inhibited bar formation, making our purely stellar models a conservative choice.

Our findings are consistent with previous simulations of LSB galaxies. L. Mayer & J. Wadsley (2004) found that bar formation requires disk masses that are at least twice those inferred for LSBs. Similar to our results, they found that LSB

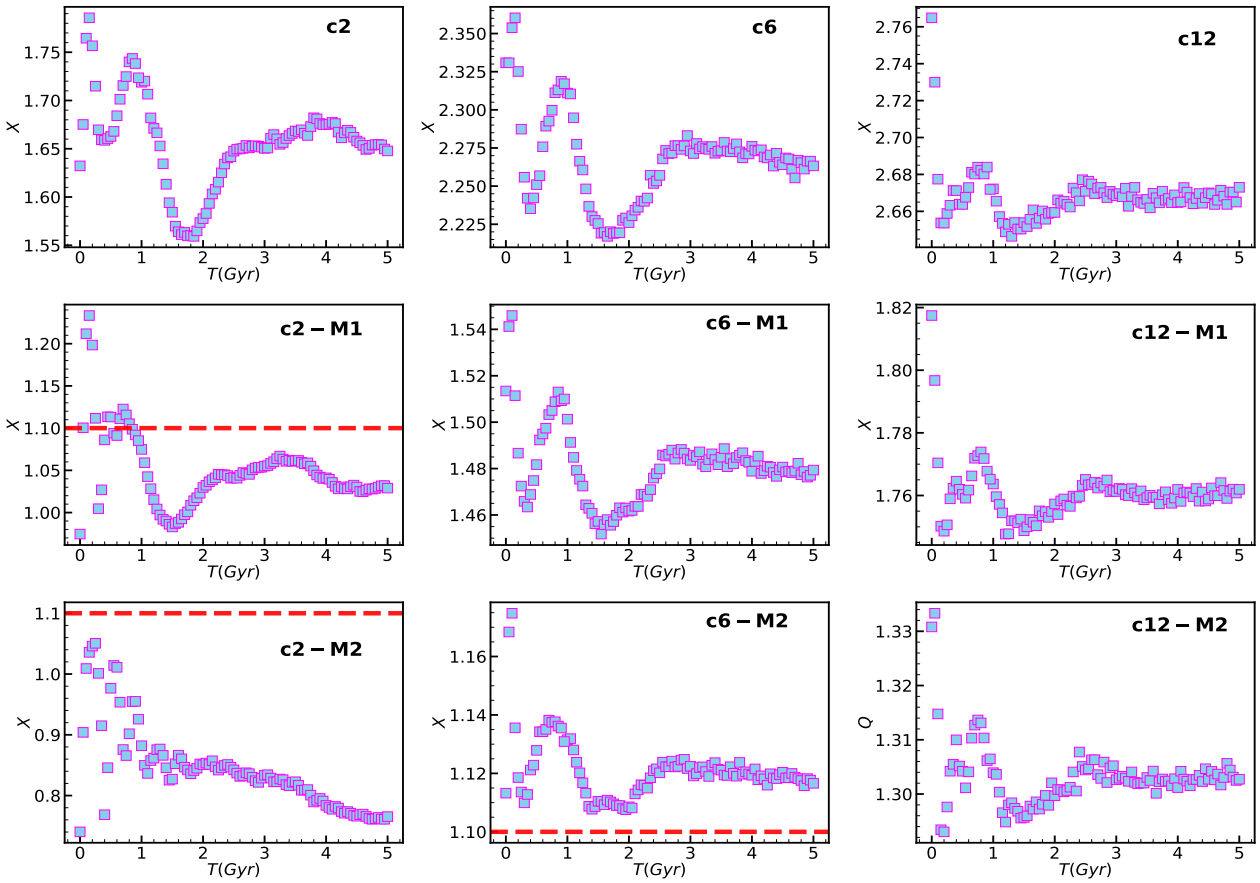

Figure 6. The time evolution of the bar instability criterion X. In the top two panels, we show the models `c2`, `c6`, and `c12`, and in the following panels, we show their massive counterparts with a higher stellar mass fraction. The horizontal line indicates the bar instability criterion: $X = 1.1$.

disks are highly stable against bar formation for a wide array of halo parameters. Interestingly, S. Ghosh et al. (2023, 2024) have shown that massive, thick stellar disks can still form bars. These results highlight the role of the stellar-to-halo mass ratio and internal disk dynamics on bar formation in N-body simulations.

We also acknowledge that other factors, such as the shape of the DM halo (spherical or triaxial) and whether the halo is live or static, can all contribute to bar formation and influence the vertical thickness (A. El-Zant & I. Shlosman 2002; I. Berentzen et al. 2006). For instance, G. Narayanan et al. (2024) propose that the quadrupole moment of the halo can drive long-lived spiral arms in LSB galaxies, while S. Hu & D. Sijacki (2016) explore the role of triaxial DM halos on spiral formation in Milky Way–like systems.

We conclude that if the ultrathin LSBs are thin, they remain so throughout their evolution in isolation regardless of the concentration of the DM halo. The LSB nature of these galaxies is paramount to their thin-disk structure. Bar formation is suppressed in these galaxies, which inhibits the internal disk heating mechanism, ensuring that LSBs maintain their relatively thin stellar disks. In contrast, their massive thin-disk counterparts with a higher stellar mass fraction residing in a shallow inner DM profile readily form bars and undergo disk thickening supported by the growth of stellar bars. Thus, our results emphasize that the LSB nature of the thin stellar disks in combination with the steep inner DM halo plays a key role in suppressing the bar formation that can otherwise heat the stellar disks.

Acknowledgments

We gratefully acknowledge the use of the high-performance computing facility “NOVA” at the Indian Institute of Astrophysics, Bengaluru, India, where all simulations were carried out. We are grateful to the anonymous referee for their careful reading and feedback which significantly improved the clarity of our paper.

ORCID iDs

K. Aditya https://orcid.org/0000-0002-1250-4359

References

Aditya, K. 2023, MNRAS, 522, 2543
Aditya, K. 2024, MNRAS, 532, 3839
Aditya, K., & Banerjee, A. 2021, MNRAS, 502, 5049
Aditya, K., Banerjee, A., Kamphuis, P., et al. 2023, MNRAS, 526, 29
Aditya, K., Kamphuis, P., Banerjee, A., et al. 2022, MNRAS, 509, 4071
Athanassoula, E. 2003, MNRAS, 341, 1179
Aumer, M., Binney, J., & Schönrich, R. 2016, MNRAS, 462, 1697
Bailin, J., Power, C., Gibson, B. K., & Steinmetz, M. 2005, arXiv:astro-ph/0502231
Banerjee, A., & Bapat, D. 2017, MNRAS, 466, 3753
Banerjee, A., & Jog, C. J. 2013, MNRAS, 431, 582
Bell, E. F., McIntosh, D. H., Katz, N., & Weinberg, M. D. 2003, ApJS, 149, 289
Berentzen, I., Shlosman, I., & Jogee, S. 2006, ApJ, 637, 582
Bizyaev, D., Kautsch, S., Sotnikova, N. Y., Reshetnikov, V. P., & Mosenkov, A. V. 2017, MNRAS, 465, 3784
Bizyaev, D., Makarov, D. I., Reshetnikov, V. P., et al. 2021, ApJ, 914, 104
Bothun, G., Impey, C., & McGaugh, S. 1997, PASP, 109, 745
Bottrell, C., Torrey, P., Simard, L., & Ellison, S. L. 2017, MNRAS, 467, 2879

Chim-Ramirez, K., Cervantes-Sodi, B., Rosas-Guevara, Y., Pérez-Montaño, L. E., & Bonoli, S. 2025, MNRAS, 539, 2262
de Grijs, R., & Peletier, R. F. 1997, A&A, 320, L21
Efstathiou, G., Lake, G., & Negroponte, J. 1982, MNRAS, 199, 1069
El-Zant, A., & Shlosman, I. 2002, ApJ, 577, 626
Ghosh, S., Fragkoudi, F., Di Matteo, P., & Saha, K. 2023, A&A, 674, A128
Ghosh, S., Fragkoudi, F., Di Matteo, P., & Saha, K. 2024, A&A, 683, A196
Ghosh, S., & Jog, C. J. 2014, MNRAS, 439, 929
Goad, J. W., & Roberts, M. S. 1981, ApJ, 250, 79
Grand, R. J., Springel, V., Gómez, F. A., et al. 2016, MNRAS, 459, 199
Haslbauer, M., Banik, I., Kroupa, P., Wittenburg, N., & Javanmardi, B. 2022, ApJ, 925, 183
Hernquist, L. 1990, ApJ, 356, 359
Hu, J., Xu, D., & Li, C. 2024, RAA, 24, 075019
Hu, S., & Sijacki, D. 2016, MNRAS, 461, 2789
Jadhav, Y. V., & Banerjee, A. 2019, MNRAS, 488, 547
Jang, D., & Kim, W.-T. 2023, ApJ, 942, 106
Jenkins, A., & Binney, J. 1990, MNRAS, 245, 305
Karachentsev, I., Karachentseva, V., & Parnovsky, S. 1993, AN, 314, 97
Karachentsev, I. D., Karachentseva, V. E., Kudrya, Y. N., Sharina, M. E., & Parnovskij, S. L. 1999, BSAO, 47, 5
Kautsch, S., Grebel, E., Barazza, F., & Gallagher, J. 2006, A&A, 445, 765
Komanduri, A., Banerjee, I., Banerjee, A., & Sengupta, S. 2020, MNRAS, 499, 5690
Lelli, F., McGaugh, S. S., & Schombert, J. M. 2016, AJ, 152, 157
Masters, K. L., Nichol, R. C., Haynes, M. P., et al. 2012, MNRAS, 424, 2180
Matthew, L., van Driel, W., & Gallagher, J. 2000, Building Galaxies; from the Primordial Universe to the Present (Paris: Frontieres), 107
Matthews, L., Gallagher III, J., & Van Driel, W. 1999, AJ, 118, 2751
Mayer, L., & Wadsley, J. 2004, MNRAS, 347, 277
McGaugh, S. S. 1996, MNRAS, 280, 337
Narayanan, G., & Banerjee, A. 2021, arXiv:2104.04216
Narayanan, G., Anagha, A. G., Banerjee, A., et al. 2024, ApJ, 973, 32
Navarro, J. F., Frenk, C. S., & White, S. D. 1997, ApJ, 490, 493
Ossa-Fuentes, L., Borlaff, A. S., Beckman, J. E., Marcum, P. M., & Fanelli, M. N. 2023, ApJ, 951, 149
Pérez-Montaño, L. E., Rodriguez-Gomez, V., Cervantes Sodi, B., et al. 2022, MNRAS, 514, 5840
Perret, V., 2016 DICE: Disk Initial Conditions Environment, Astrophysics Source Code Library, ascl:1011.007
Pillepich, A., Springel, V., Nelson, D., et al. 2018, MNRAS, 473, 4077
Ramirez, K. C., Sodi, B. C., Rosas-Guevara, Y., Pérez-Montaño, L. E., & Bonoli, S. 2025, arXiv:2504.02145
Romeo, A. B., & Falstad, N. 2013, MNRAS, 433, 1389
Romeo, A. B., Agertz, O., & Renaud, F. 2023, MNRAS, 518, 1002
Saha, K. 2014, arXiv:1403.1711
Saha, K., Tseng, Y.-H., & Taam, R. E. 2010, ApJ, 721, 1878
Schaye, J., Crain, R. A., Bower, R. G., et al. 2015, MNRAS, 446, 521
Sellwood, J. 2013, ApJL, 769, L24
Sellwood, J. 2016, ApJ, 819, 92
Sellwood, J., & Gerhard, O. 2020, MNRAS, 495, 3175
Sellwood, J. A., & Evans, N. W. 2001, ApJ, 546, 176
Sharma, S., Bland-Hawthorn, J., Binney, J., et al. 2014, ApJ, 793, 51
Sodi, B. C., & García, O. S. 2017, ApJ, 847, 37
Sotillo-Ramos, D., Donnari, M., Pillepich, A., et al. 2023, MNRAS, 523, 3915
Toomre, A. 1964, ApJ, 139, 1217
Fall, S. M., & Lynden-Bell, D. 1981, in Proceedings of a NATO Advanced Study Institute at the Institute of Astronomy and Clare College (Cambridge: Cambridge Univ. Press), 111
Vogelsberger, M., Genel, S., Springel, V., et al. 2014, MNRAS, 444, 1518
Weinberger, R., Springel, V., & Pakmor, R. 2020, ApJS, 248, 32
Xu, D., Gao, H., Bottrell, C., Yesuf, H. M., & Shi, J. 2024, ApJ, 974, 88
Zhou, Z., Ma, J., & Wu, H. 2021, AJ, 161, 260